Journal of Molecular Spectroscopy **196,** 29–44 (1999)
Article ID jmsp.1999.7849, available online at http://www.idealibrary.com on IDEAL®

The BaI $X^2\Sigma^+$ and $B^2\Sigma^+$ Electronic States Through $B^2\Sigma^+$–$X^2\Sigma^+$ and $C^2\Pi$–$X^2\Sigma^+$ Band Systems Analysis

R. F. Gutterres,*,†,‡ J. Vergès,* and C. Amiot*

*Laboratoire Aimé Cotton, C.N.R.S. II Université Paris Sud, Bât. 505, Campus d'Orsay 91405, Orsay Cedex, France; †Laboratório de Espectroscopia e Laser, Universidade Federal Fluminense, Campus da Boa Viagem, Niterói, RJ 24210-340, Brazil; and ‡Bolsista CAPES, Brasília, Brazil

E-mail: amiot@lx4.lac.u-psud.fr

Received November 9, 1998; in revised form February 26, 1999

The near-infrared spectrum of the $B^2\Sigma^+$–$X^2\Sigma^+$ band system of the BaI molecule, obtained from the chemiluminescent reaction Ba + I_2 and also by laser-induced fluorescence (LIF), was recorded by using Fourier transform spectroscopy (FTS). The LIF spectra were obtained by using a Ti:sapphire single-mode laser excitation. Resolved rotational data, originating from 32 vibrational levels ($0 \le v \le 31$) in the $X^2\Sigma^+$ state and from 24 vibrational levels ($0 \le v \le 19$, and $v = 21, 22, 23, 26$) in the $B^2\Sigma^+$ state, were used in the final analysis. Previously recorded data for the $C^2\Pi$–$X^2\Sigma^+$ band system (with $\Delta v = 0$), taken from C. A. Leach, A. A. Tsekouras, and R. N. Zare, *J. Mol. Spectrosc.* **153,** 59–72 (1992), were added to the present work data field. Accurate and improved molecular constants for the $X^2\Sigma^+$, $B^2\Sigma^+$, and $C^2\Pi$ states were derived from a simultaneous treatment of the whole data set.

Key Words: Fourier transform spectroscopy; laser-induced fluorescence; BaI *B–X* band system; molecular constants.

I. INTRODUCTION

The alkaline–earth monohalides *MX* (where *M* is the metal and *X* the halogen) have attracted the interest of theoretical and experimental spectroscopists for decades. These molecules are highly ionic compounds and have nine valence electrons outside closed shells. The structure of the ground electronic state and the structures of the first excited electronic states can be described by an unpaired electron and a molecular ion core consisting of two closed shell ions M^{2+} and X^-. From this theoretical approach it is expected that the electronic structure of the alkaline–earth monohalides should have a behavior similar to the one of the alkali atoms, and the electronic states $A'^2\Delta$, $A^2\Pi$, $B^2\Sigma^+$, and $C^2\Pi$ would be formed from the excitation of the unpaired *ns* electron to the low-lying $(n-1)$ states. Different ionic bonding models have been developed to represent the structure of these first excited states, e.g., the electrostatic polarization model (*2, 3*) and the ligand–field approach (*4*). From these models, predictions of both the transition energies and the permanent and transition dipole moments have been made for several alkaline–earth monohalide molecules, including the BaI molecule (*5, 6*).

Up until this moment, all experimental spectroscopic studies with rotational resolution of the BaI molecule have concerned the $C^2\Pi$–$X^2\Sigma^+$ electronic system and have always been done with $\Delta v = 0$ vibrational transitions.

The first observation of vibrational bands was made in 1928 by Walters and Barratt (*7*). Later, Mesnage (*8*) studied the $C^2\Pi$–$X^2\Sigma^+$ bandheads and more detailed vibrational analyses of this band system have been performed by Patel and Shah (*9*) and Rao *et al.* (*10*). In their work, Patel and Shah (*9*) have also recognized that the absorption spectrum in the region of 380 nm observed by Walters and Barratt (*7*) was caused by two other electronic band systems, $E^2\Sigma^+$–$X^2\Sigma^+$ at about 374 nm and $D^2\Sigma^+$–$X^2\Sigma^+$ at about 388 nm. Bradford *et al.* (*11*) have observed the chemiluminescence reaction Ba + I_2 and determined that the infrared emission was issued from two unobserved electronic transitions, $A^2\Pi$–$X^2\Sigma^+$ and $B^2\Pi$–$X^2\Sigma^+$. In all previously mentioned works, the experiments were unable to resolve the individual rotational transitions which are very closely spaced, mainly because of the fact that the large mass of barium and iodine atoms results in very small rotational constants.

However, there has been a high accuracy systematic study of the $C^2\Pi$–$X^2\Sigma^+$ band system with rotational resolution since 1981. Using population-labeling optical–optical double resonance (PLOODR), Johnson *et al.* (*12*) and Johnson and Zare (*13*) have assigned the $C^2\Pi$–$X^2\Sigma^+$ (0–0) band, and the same band has been studied also by using selectively detected laser-induced fluorescence (SDLIF) by Johnson *et al.* (*14*). In the last three cited works, a collimated beam of the BaI molecule obtained from an oven source was used and the molecular constants for the $C^2\Pi$ and $X^2\Sigma^+$ states were calculated. It must also be emphasized that the determined molecular constants in the last three mentioned works were found to be essentially equal to each other. Nevertheless, using a crossed-beam apparatus, SDLIF, and laser-induced fluorecence (LIF), Zhao *et al.* (*15*) have performed a powerful study of the $C^2\Pi$–$X^2\Sigma^+$ (0–0) band in which high rotational levels (J'' up to nearly

0022-2852/99 $30.00

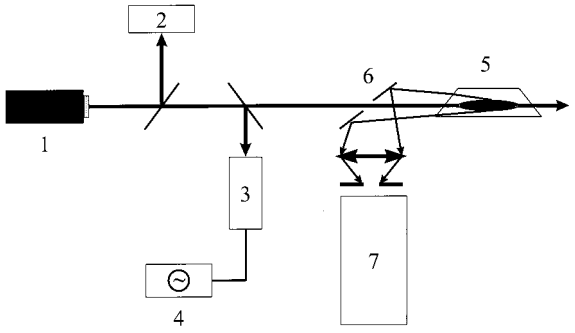

FIG. 1. Scheme of the experimental setup. (1) Laser source (Ti:Sa laser); (2) lambdameter; (3) Fabry–Perot spectrum analyzer; (4) oscilloscope recording the transmission fringes of the spectrum analyzer; (5) Heat pipe oven; (6) Pierced mirror collecting the fluorescence light backward with respect to the laser beam; (7) 2-m optical path length Fourier transform spectrometer. Devices 1, 2, 3, and 4 are not used in the recording of the chemiluminescent spectrum.

500) were observed. From this data set, and combining with previous results (*12–14*), it was possible for the authors to determine an improved and more general set of molecular constants. Using PLOODR, Leach *et al.* (*16*) have observed and assigned the $C^2\Pi$–$X^2\Sigma^+$ (8–8) band. Finally, Leach *et al.* (*1*) have performed a general rovibrational analysis of the BaI $C^2\Pi$–$X^2\Sigma^+$ band system with $v \leq 12$. The observed bands ($\Delta v = 0$), with $v = 0$, 1, 4, 8, and 12, were recorded by SDLIF, and, in addition, the bands ($\Delta v = 0$), with $v = 0$, 1, 2 and 3, were measured by LIF, in which undispersed fluorescence was detected. The obtained data were combined with previous results (*14*, *13*, *16*) and also with microwave measurements of low J'' for $v = 0$–5 of the $X^2\Sigma^+$ state obtained by Töring and Döbl (*17*). A set of 31 molecular constants was derived from a weighted nonlinear fit and it reproduced the 5032 observed transition wavenumbers with a standard deviation of 2.37×10^{-3} cm^{-1}. In the final description of the Hamiltonian, the pure vibrational terms were defined as follows,

$$\begin{aligned} \Delta\nu &= T'_e - T''_e + Y'_{00} - Y''_{00} \\ \Delta\omega_e &= \omega'_e - \omega''_e \\ \Delta\omega_e x_e &= \omega_e x'_e - \omega_e x''_e, \end{aligned} \qquad [1]$$

and the values obtained for these constants by the authors strongly improved the values obtained by Rao *et al.* (*10*).

More than 2400 observed wavenumbers of the $B^2\Sigma^+$–$X^2\Sigma^+$ band system were assigned in the present work. The LIF near-infrared spectra, obtained from the Ti:sapphire single-mode laser excitation, were recorded by using Fourier transform spectroscopy (FTS). The highly congested spectrum of the $B^2\Sigma^+$–$X^2\Sigma^+$ (0, 0) band, obtained from the chemiluminescent reaction Ba + I_2, was also recorded by using FTS. Resolved rotational data, originating from 32 vibrational levels ($0 \leq v \leq 31$) in the $X^2\Sigma^+$ state and from 24 vibrational levels ($0 \leq v \leq 19$, and $v = 21$, 22, 23, 26) in the $B^2\Sigma^+$ state, have permitted a first analysis of the observed transitions. A set of 27 constants was calculated and reproduced the observed wavenumbers with a standard deviation similar to the one obtained in (*1*). In this way, the spectral data set obtained by Leach *et al.* (*1*) could be included in a second global analysis including both the $B^2\Sigma^+$–$X^2\Sigma^+$ and the $C^2\Pi$–$X^2\Sigma^+$ band systems.

TABLE 1
Vacuum Wavenumber σ and Emitted Power P of the Used Ti:Sapphire Laser Radiations

σ (cm^{-1})	P (W)	σ (cm^{-1})	P (W)	σ (cm^{-1})	P (W)
10042.86	0.3	10393.95	0.3	10695.23	0.4
10056.79	0.2	10394.52	0.4	10726.83	1.0
10100.22	0.3	10422.82	0.4	10822.36	0.4
10150.27	0.4	10422.89	0.3	10837.34	1.0
10200.50	0.4	10436.81	0.4	10869.46	1.1
10257.79	0.2	10501.80	0.4	10927.96	1.1
10350.79	1.0	10530.22	0.4	10933.50	1.1
10372.34	1.0	10558.81	0.4	10977.34	1.1
10372.43	1.0	10652.12	0.4	10977.70	1.1

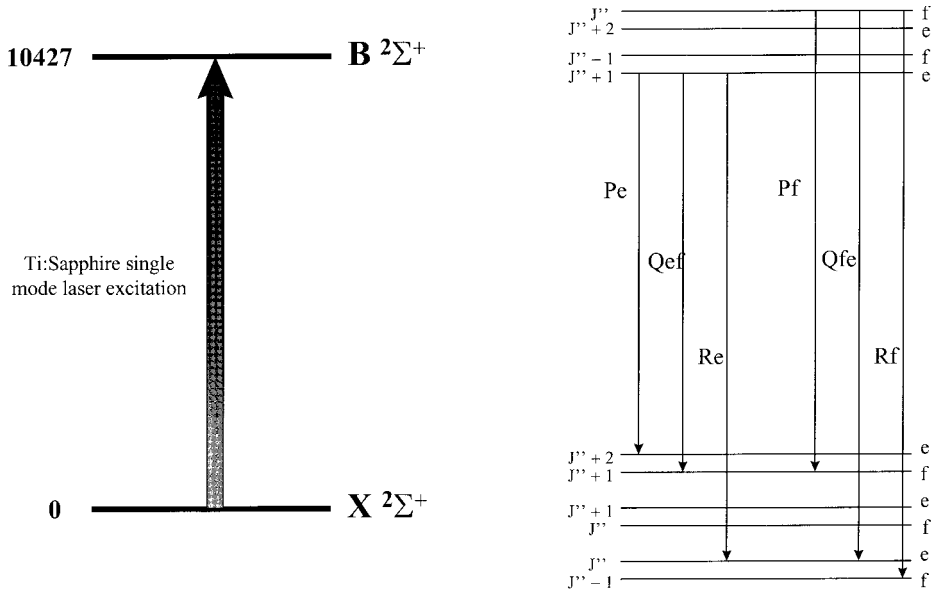

FIG. 2. Energy level scheme of the *B–X* transition.

The several observed transitions with $\Delta v \neq 0$ have permitted the solution of pure vibrational terms described in terms of Eq. [1]. A set of 51 molecular constants was calculated and reproduced both the observed $B^2\Sigma^+ - X^2\Sigma^+$ and the $C^2\Pi - X^2\Sigma^+$ band systems spectral data, with a standard deviation less than 2.3×10^{-3} cm^{-1}.

II. THE EXPERIMENT

A heat pipe oven was used for the production of the BaI molecules. This molecular source was proposed by Vidal and Cooper (*18*) and has been largely used in experimental studies of alkaline–earth monohalides like BaCl (*19–22*),

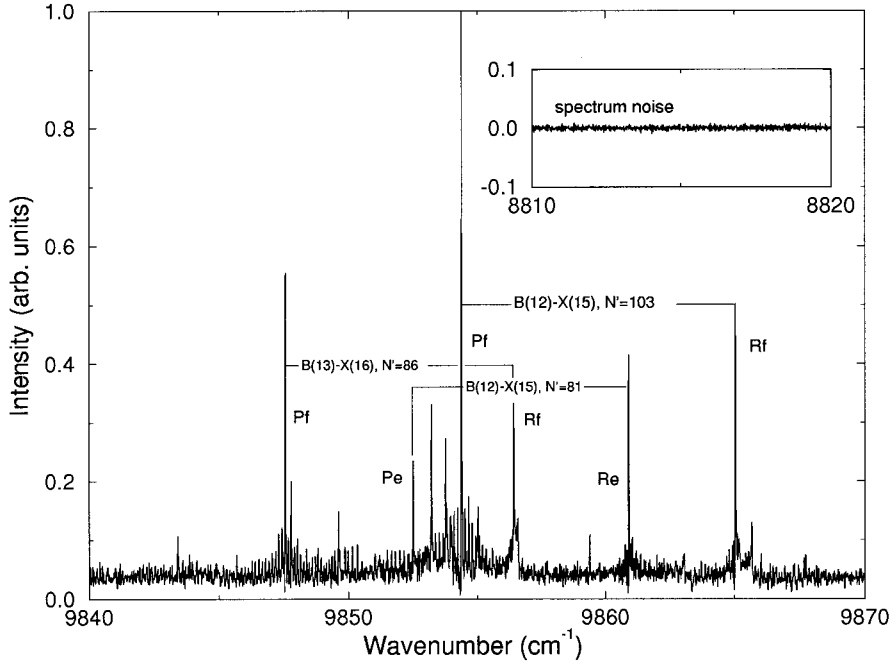

FIG. 3. Part of the *B–X* LIF spectrum induced by a Ti:sapphire 920.01-nm laser line. Numbers in parentheses are the v'' values of the transitions. Inset shows the spectrum noise.

TABLE 2

Ti:Sapphire Single-Mode Laser Wavelength σ, Quantum Numbers v', J', and Energy E' for the $B^2\Sigma^+$ Excited State, Quantum Numbers v'', J'', and Energy E'' of the Lower Level in the Ground $X^2\Sigma^+$ state

$\sigma(cm^{-1})$	v'	J'	$E'(cm^{-1})$	v''	J''	$E''(cm^{-1})$	Δv
10042.86	8	41.5	11660.127	10	42.5	1617.263	5-7
	6	130.5	11769.692	8	131.5	1726.828	4-8
	7	157.5	12103.390	8	156.5	2060.526	4-7
10056.79	7	87.5	11678.076	9	86.5	1621.287	4-6
	7	44.5	11529.713	9	83.5	1472.924	4-6
	5	110.5	11509.489	7	111.5	1452.700	2-4
10100.22	2	59.5	10870.211	4	58.5	769.998	0-4
	2	17.5	10789.503	4	18.5	689.280	0-4
10150.27	8	228.5	12952.589	9	229.5	2852.366	5-11
	8	228.5	12952.589	9	229.5	2852.366	5-11
10200.50	6	111.5	11664.738	7	112.5	1464.238	2-10
	7	26.5	11495.617	8	27.5	1295.117	3-5
	7	132.5	11933.911	8	131.5	1733.411	3-9
	7	62.5	11573.622	8	61.5	1373.162	3-10
	4	233.5	12449.090	5	232.5	2248.590	1-7
	0	309.5	12987.663	1	310.5	2787.163	0-1
	2	222.5	12049.144	3	223.5	1848.644	0-5
10257.79	1	87.5	10835.767	2	86.5	577.977	0-4
	1	155.5	11278.552	2	154.5	1020.762	0-4
	0	160.5	11162.910	1	159.5	905.120	0-2
10350.79	7	90.5	11691.939	7	89.5	1341.149	4-9
	6	178.5	12165.216	6	177.5	1714.426	3-8
	3	186.5	11810.411	3	187.5	1459.621	1-6
	1	240.5	12124.978	1	241.5	1774.188	1-4
	1	274.5	12600.349	1	275.5	2249.559	1-4
10372.34	2	218.5	12004.117	2	217.5	1631.773	0-4
	0	247.5	12101.752	0	248.5	1729.408	0-2
10372.43	18	72.5	13084.215	17	73.5	2711.785	13-15
	1	184.5	11515.341	1	185.5	1142.911	0-4
	2	184.5	11673.515	2	185.5	1301.085	0-5
	1	251.5	12263.089	1	250.5	1890.659	0-4

Note. Δv represents the range of observed v values in the $X^2\Sigma^+$ state.

TABLE 2—*Continued*

$\sigma(cm^{-1})$	v'	J'	$E'(cm^{-1})$	v''	J''	$E''(cm^{-1})$	Δv
10393.95	1	110.5	10953.243	1	111.5	559.294	0-4
	1	141.5	11169.963	1	142.5	776.014	0-4
	0	150.5	11082.614	0	149.5	688.665	0-1
	2	120.5	11012.822	2	119.5	618.873	0-5
	1	224.5	11958.870	1	223.5	1564.921	0-4
10394.52	1	173.5	11414.127	1	172.5	1019.603	0-4
	2	116.5	11128.195	2	115.5	733.671	0-5
	0	147.5	11059.523	0	148.5	664.999	0-2
10422.82	0	105.5	10796.285	0	104.5	373.470	0-3
	0	101.5	10774.435	0	100.5	351.365	0-2
	6	279.5	13311.608	5	280.5	2888.793	3-8
	4	320.5	13662.648	3	321.5	3240.621	2-6
10422.89	0	104.5	10790.745	0	103.5	367.860	0-3
10436.81	6	252.5	12951.247	5	253.5	2514.439	2-10
	2	364.5	14190.799	1	365.5	3753.991	0-5
	8	232.5	12999.215	7	233.5	2562.407	3-12
	11	128.5	12448.342	10	129.5	2011.534	6-15
	5	333.5	14006.110	4	332.5	3569.302	2-9
	4	389.5	14919.900	3	388.5	4483.092	2-7
	9	269.5	13598.807	8	268.5	3161.999	6-13
	1	382.5	14397.189	0	383.5	3960.381	0-4
	12	198.5	13139.448	11	197.5	2702.640	11-21
10501.80	6	79.5	11505.870	5	80.5	1004.091	2-9
	5	135.5	11680.840	4	136.5	1179.061	1-8
	4	146.5	11607.798	3	147.5	1106.019	1-7
	2	238.5	12262.677	1	239.5	1760.898	0-5
10530.22	3	105.5	11216.207	2	106.5	685.992	0-6
	2	153.5	11401.491	1	154.5	871.276	0-5

BaBr (*23*), BaF (*24, 25*), and CaF (*26*). In the recording of the LIF spectra, a mixture of a few grams of Ba metal and BaI_2 powder was heated to 850°C in the presence of 12 mbar of argon buffer gas. In the chemiluminescent spectrum obtention, the same compound was heated to 1200°C in the presence of 60 mbar of argon buffer gas. The obtained fluorescence in both cases (LIF and chemiluminescent spectra) was focused into the entrance iris of a 2-m optical path

TABLE 2—*Continued*

$\sigma(cm^{-1})$	v'	J'	$E'(cm^{-1})$	v''	J''	$E''(cm^{-1})$	Δv
10558.81	1	39.5	10678.768	0	40.5	119.959	0-3
	1	145.5	11199.967	0	144.5	561.158	0-4
	1	93.5	10863.781	0	92.5	304.972	0-4
	8	305.5	13953.575	7	304.5	3394.766	4-11
10652.12	16	198.5	13663.288	13	197.5	3011.168	11-20
	15	205.5	13624.277	12	206.5	2972.157	10-19
	11	300.5	14313.939	8	301.5	3661.819	6-15
	3	203.5	12011.901	1	204.5	1359.781	0-6
10695.23	15	74.5	12695.484	12	73.5	2000.259	10-20
	12	191.5	13091.665	9	193.5	2396.440	7-17
	11	220.5	13259.877	8	221.5	2564.652	6-16
	2	64.5	10886.134	0	65.5	190.909	0-4
	9	294.5	13920.425	6	293.5	3225.200	5-13
	10	301.5	14184.799	7	300.5	3489.574	6-14
	6	331.5	14138.237	3	332.5	3443.012	3-9
10726.83	11	111.5	12332.426	8	112.5	1605.597	6-15
	10	148.5	12439.390	7	149.5	1712.561	5-14
	9	179.5	12560.484	6	180.5	1833.655	4-13
	7	257.5	13175.651	4	258.5	2448.822	3-11
	18	260.5	14641.664	14	261.5	3914.835	12-22
	6	305.5	13691.642	3	304.5	2964.831	3-8
	18	67.5	13067.020	14	68.5	2414.900	21-22
	6	49.5	11399.009	4	50.5	686.889	2-9
	6	99.5	11588.367	4	100.5	936.247	2-10
	4	198.5	12065.162	2	199.5	1413.062	1-7
10822.36	14	194.5	13363.588	10	193.5	2541.227	9-19
	16	139.5	13186.463	12	138.5	2364.102	10-21
	15	112.5	12871.674	11	113.5	2049.313	10-20
	14	171.5	13173.136	10	172.5	2350.775	8-19
	12	252.5	13693.615	8	251.5	2871.254	8-17
	4	67.5	11182.840	1	68.5	360.479	1-7

TABLE 2—*Continued*

$\sigma(cm^{-1})$	v'	J'	$E'(cm^{-1})$	v''	J''	$E''(cm^{-1})$	Δv
10837.34	26	61.5	14087.444	21	62.5	3250.103	19-31
	23	235.5	14969.209	18	234.5	4113.868	16-28
	15	95.5	12783.993	11	94.5	1946.652	9-20
	15	129.5	12987.262	11	128.5	2149.921	9-20
	15	53.5	12628.925	11	94.5	1791.584	9-20
	14	105.5	12701.149	10	106.5	1863.808	9-19
	12	174.5	12916.584	8	175.5	2079.243	7-17
	3	101.5	11183.565	0	100.5	346.224	0-6
10869.46	12	102.5	12429.383	8	103.5	1559.921	7-17
	13	85.5	12481.710	9	84.5	1612.348	7-17
	12	82.5	12325.982	8	83.5	1559.921	8-16
	22	165.5	14142.047	17	164.5	3272.585	16-26
	21	199.5	14315.502	16	198.5	3446.040	16-25
	13	40.5	12331.477	9	39.5	1462.015	9-17
10927.96	19	102.5	13343.815	14	101.5	2415.864	13-24
	6	139.5	11831.450	2	140.5	903.491	3-9
	19	132.5	13530.400	14	131.5	2602.441	13-24
	17	147.5	13359.381	12	148.5	2431.442	11-22
	16	220.5	13889.624	11	219.5	2961.665	10-21
	6	219.5	12582.210	2	218.5	1654.251	3-9
10933.50	19	70.5	13208.123	14	69.5	2274.627	13-24
	17	133.5	13262.503	12	134.5	2329.007	12-22
	14	218.5	13608.452	9	69.5	2674.956	9-18
	19	103.5	13359.681	14	104.5	2426.185	13-23
	8	28.5	11632.808	4	27.5	699.312	4-12
	7	100.5	11741.750	3	101.5	808.254	3-11
	6	171.5	12084.077	2	170.5	1150.581	4-9
10977.34	14	165.5	13105.017	9	164.5	2127.342	9-19
	15	121.5	12923.884	10	120.5	1946.540	10-19

length Fourier transform spectrometer. A scheme of the experimental setup is shown in Fig. 1.

A total of 27 laser lines, provided by a Ti:sapphire single-mode laser (Coherent 899-21), were used to excite the molecules in the LIF spectra obtention. The stability of the laser, in both intensity and frequency, was sufficiently high during the

TABLE 2—*Continued*

$\sigma(cm^{-1})$	v'	J'	$E'(cm^{-1})$	v''	J''	$E''(cm^{-1})$	Δv
10977.34	16	28.5	12711.242	11	27.5	1733.898	12-20
	14	123.5	12803.634	9	124.5	1826.290	9-18
	15	99.5	12813.824	10	100.5	1836.480	10-19
	14	144.5	12958.663	9	145.5	1981.319	9-18
10977.70	14	143.5	12951.407	9	144.5	1973.712	9-18
	16	13.5	12695.947	11	12.5	1718.252	11-20
	13	178.5	13102.837	8	179.5	2125.142	8-17

recording time. Table 1 shows the spectral characteristics, vacuum wavenumber, and emitted power of all used Ti:sapphire laser lines.

The recording time of the interferograms was about 2 h. The fluorescence spectra were recorded in the region between 9000 and 12 000 cm^{-1} with an unapodized resolution limit ranging from 0.005 to 0.02 cm^{-1}. The wavenumbers were calibrated relative to a fixed frequency reference line (Xe atomic transition near 3.5 μm) used to monitor the path difference in the interferometer. The absolute measurement uncertainties varied from 1×10^{-3} cm^{-1} for the strongest lines to 5×10^{-3} cm^{-1} for the weakest ones.

III. RESULTS

The main characteristic of the obtained spectra is their complexity. The observed $B^2\Sigma^+$–$X^2\Sigma^+$ band system involves two doublet states and each vibrational band contains four observed rotational branches. In addition, the large mass of barium and iodine atoms results in small rotational constants and consequently the spectra are highly congested. Figure 2 shows an energy level scheme for the $B^2\Sigma^+$–$X^2\Sigma^+$ transition.

(a) The LIF Spectra

The LIF technique permits the selection of a smaller number of coincident laser and molecular line transitions.

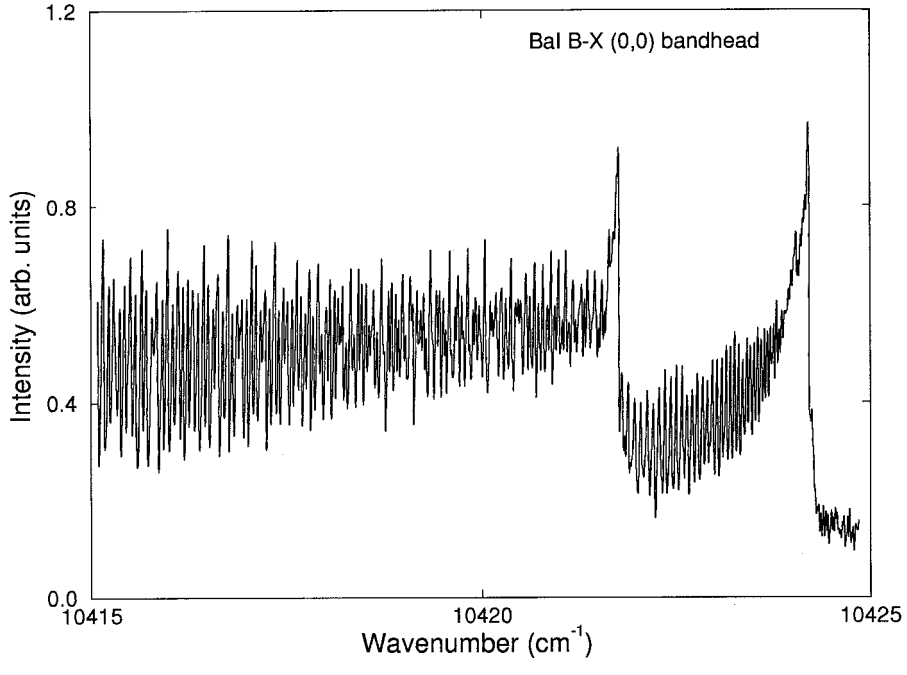

FIG. 4. Part of the chemiluminescent spectrum of the B–X (0, 0) band system.

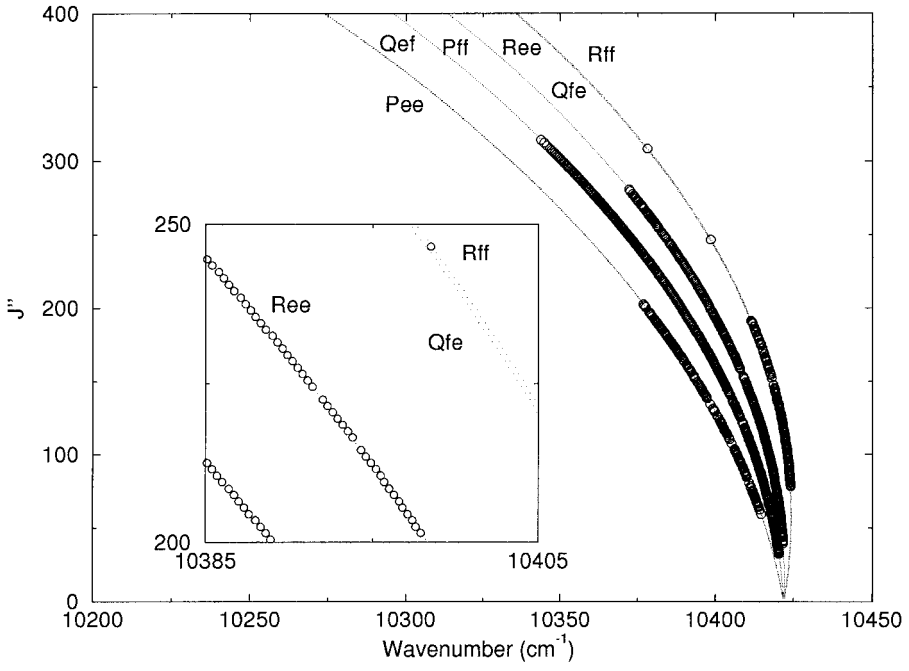

FIG. 5. Fortrat diagram of the B–X (0, 0) band system. The points represented by (○) are the observed energy levels and correspondent wavenumbers, the dotted points are obtained from the determined molecular constants. Inset shows the observed and calculated energy levels in detail.

Consequently, the spectra are less dense than in the classical emission where a great number of upper excited levels are involved. Therefore, the assignment of quantum numbers to the observed transitions is relatively simpler than in the classical case. Several doublets can be observed in Fig. 3, which shows a part of the recorded LIF spectra. Each line is surrounded by collisional rotational relaxation lines; their intensities decreasing regularly and rapidly. As has been observed by Hafid *et al.* (*21*) in the BaCl molecule, the intensities of the P and R line doublets, connected with

TABLE 3
Hamiltonian Energy Matrix for the Isolated $C^2\Pi$ Electronic State

	$^2\Pi_{3/2}$	$^2\Pi_{1/2}$
$^2\Pi_{3/2}$	$T + A/2 + (B + A_J)(X-1)$ $- D[(X-1)^2 + X]$ $+ H[(X-1)^3 + X(3X-1)]$ $+ (A_{JJ}/2)[3(X-1)^2 + X] + (q/2)X$	$- BX^{1/2} + 2DX^{3/2}$ $- HX^{1/2}(3X^2 + X + 1) + A_{JJ}X^{1/2}$ $+ (q/2)[X^{1/2}[-1 \pm (X+1)^{1/2}]]$ $- (p/4)X^{1/2}$
$^2\Pi_{1/2}$	sym.	$T - A/2 + (B + A_J)(X-1)$ $- D[(X+1)^2 + X]$ $+ H[(X+1)^3 + X(3X+1)]$ $- (A_{JJ}/2)[3(X+1)^2 + X]$ $+ (q/2)[X + 2 \mp 2(X+1)^{1/2}]]$ $+ (p/2)[1 \mp (X+1)^{1/2}]$

Note. $X = (J + \frac{1}{2})^2 - 1$. Matrix elements are calculated using an *e*/*f* parity basis and are written *e* over *f*.

TABLE 4

Molecular Constants in cm^{-1} for the $X^2\Sigma^+$ and $B^2\Sigma^+$ Electronic States Determined in a Preliminary Analysis from a Nonlinear Least-Squares Fit of the Fourier Spectroscopy Data Set

coeff.	$X^2\Sigma^+$	$B^2\Sigma^+$
T_e	[0]	10427.02222(43)[1]
$B_e \times 10^{+2}$	2.6805248(840)	2.6114207(842)
$D_e \times 10^{+9}$	3.3100(139)	3.5189(140)
$H_e \times 10^{+16}$	-2.237(634)	-3.314(638)
$\alpha_B \times 10^{+5}$	6.63677(103)	7.23994(133)
$\beta_B \times 10^{+8}$	3.4893(615)	4.7233(998)
$\gamma_B \times 10^{+11}$	7.16(151)	15.41(221)
$\alpha_D \times 10^{+12}$	1.4598(540)	2.5520(881)
$\beta_D \times 10^{+14}$	-	-3.307(496)
ω_e	152.163523(292)	141.951571(323)
$\omega_e x_e$	0.2726932(211)	0.2896352(271)
$\omega_e y_e \times 10^{+4}$	2.37586(509)	3.10775(692)
$\gamma_e \times 10^{+3}$	2.643(202)	-56.302(202)
$\gamma_J \times 10^{+8}$	-	1.21118(429)
$\gamma_v \times 10^{+5}$	-1.1938(514)	8.1727(544)

Note. Numbers in parentheses represent two standard deviations in units of the last figure quoted.

[1] Origin of the energies at the level $v = -\frac{1}{2}$, $N = 0$ of the ground state ($T_e = 0$). Same origin is in Table 5.

upper rotational levels of *e* or *f* symmetry levels, are different. When the pumped rovibrational level of the $B^2\Sigma^+$ electronic state has a type-*e* symmetry, the R_e line is stronger than the P_e one, but when the pumped level has a type-*f* symmetry, the P_f line is stronger than the R_f. The thermal emission produced by the chemiluminescent reaction Ba + I_2 can also be seen in Fig. 3. This emission is noted in the most of the LIF spectra and the spectra noise is also shown in Fig. 3.

Several fluorescence progressions have been observed. Table 2 lists the quantum numbers J', v', and the energy term value E' of the involved $B^2\Sigma^+$ level together with the quantum numbers J'', v'', and the energy term value E'' of the lower level in the ground $X^2\Sigma^+$ state. The table shows also the range of observed vibrational levels in the $X^2\Sigma^+$ state. All the line wavenumbers were assigned to transitions involving vibrational levels up to $v' = 26$ in the $B^2\Sigma^+$ state and $v'' = 31$ in the $X^2\Sigma^+$ state.

(b) The Chemiluminescent Spectrum

The spectrum of the $B^2\Sigma^+$–$X^2\Sigma^+$ (0, 0) band, obtained from the chemiluminescent reaction Ba + I_2, is highly congested and the typical separation between the observed lines is lower than 0.01 cm^{-1}. A part of the recorded spectrum can be seen in Fig. 4.

The observed spectral high density of the chemiluminescent spectrum is a consequence both of the very similar potential curves for the two states ($B^2\Sigma^+$ and $X^2\Sigma^+$), which have similar vibrational (and rotational) constants, and of the doublet structure of the involved transition. The separation of the vibrational bands with the same Δv (for low vibrational levels) is only about 10 cm^{-1} and the overlap in the spectrum of the band systems with the same Δv is severe. In addition, the doublet structure of the involved states has, as a consequence, the splitting of each vibrational band in six overlapping rotational branches (of which two have not been observed in the obtained spectra). Figure 5 shows a Fortrat diagram of the

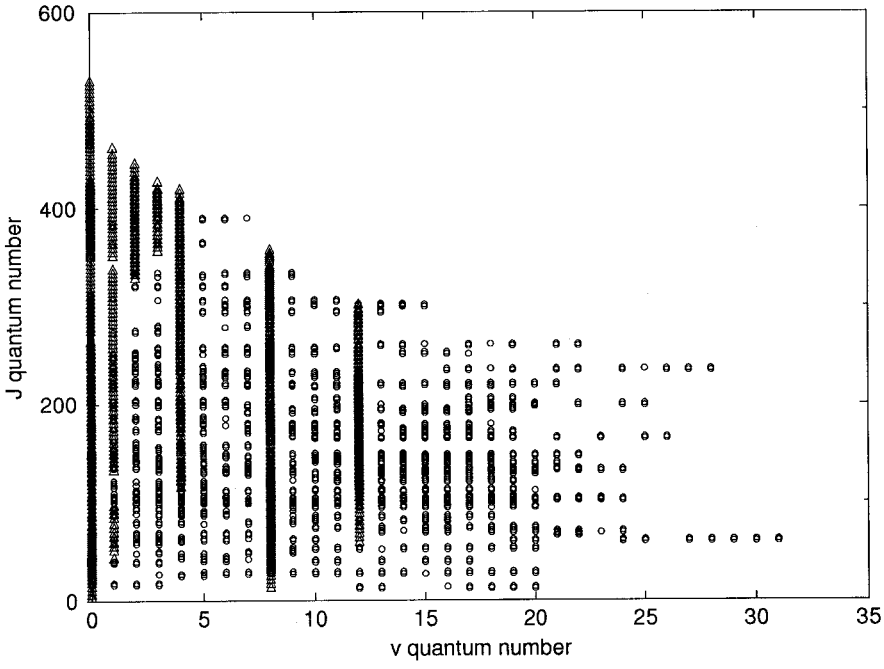

FIG. 6. Schematic representation of the $X^2\Sigma^+$ data set used in the reduction of wavenumbers to the molecular constants. (○) represents the observed levels and (△) reprents the data obtained from (*1*).

$B^2\Sigma^+$–$X^2\Sigma^+$ (0, 0) band system with the observed lines pointed.

Numerous bands other than the $B^2\Sigma^+$–$X^2\Sigma^+$ (0–0) were observed in the chemiluminescent spectrum. Their small intensities and strong overlaps prevent including the corresponding spectral data in the global calculations.

IV. ANALYSIS

In a first step, all available spectroscopic data of the $B^2\Sigma^+$–$X^2\Sigma^+$ band system, obtained from the LIF spectra and the chemiluminescent spectrum (0–0 band), were reduced by using a nonlinear least-squares method. Both energy term values

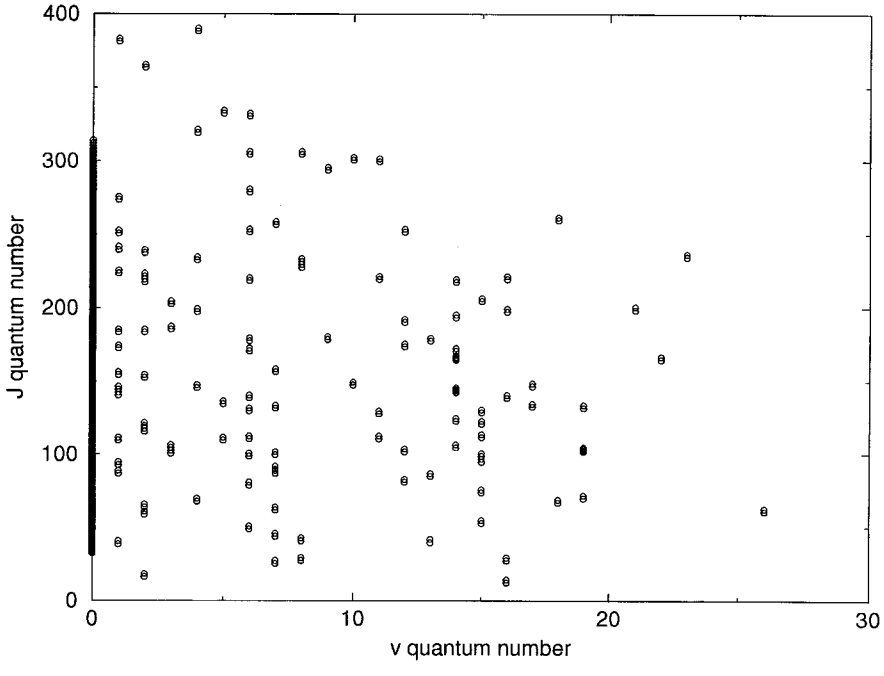

FIG. 7. Schematic representation of the $B^2\Sigma^+$ data set used in the reduction of wavenumbers to the molecular constants.

TABLE 5

Molecular Constants in cm^{-1} for the $X^2\Sigma^+$, $B^2\Sigma^+$, and $C^2\Pi$ Electronic States Determined in the Final Analysis from a Nonlinear Least-Squares Fit of the Global Data Set

coeff.	$X^2\Sigma^+$(a)	$X^2\Sigma^+$(b)	$B^2\Sigma^+$(a)	$C^2\Pi$(a)	$C^2\Pi$(b)
T_e	[0]	-	10427.02214(43)	18188.49572(32)	-
$B_e \times 10^{+2}$	2.6805603(479)	2.6805878(8)	2.6114569(480)	2.6727975(489)	2.672800(17)
$D_e \times 10^{+9}$	3.32258(449)	3.3288(10)	3.53151(454)	3.06861(462)	3.0726(14)
$H_e \times 10^{+16}$	-1.422(171)	-1.272(80)	-2.510(173)	-1.191(172)	-1.032(80)
$\alpha_B \times 10^{+5}$	6.6637046(989)	6.6342(3)	7.24092(131)	6.362327(968)	6.3610(22)
$\beta_B \times 10^{+8}$	3.5181(563)	3.397(32)	4.8150(592)	2.8178(373)	2.50(5)
$\gamma_B \times 10^{+11}$	6.26(138)	-	13.56(221)	-	-
$\alpha_D \times 10^{+12}$	1.4659(525)	1.31(29)	2.4777(913)	1.7532(547)	1.693(295)
$\beta_D \times 10^{+14}$	-	-	-0.2728(546)	-	1.06(22)
$A_e \times 10^{-2}$	-	-	-	7.56059476(474)	7.560594(5)
$A_J \times 10^{+6}$	-	-	-	-4.0420(133)	-4.0716(108)
$A_{JJ} \times 10^{+12}$	-	-	-	4.7255(438)	7.253(51)
$A_v \times 10^{+1}$	-	-	-	1.09401(148)	1.09045(148)
$A_{vv} \times 10^{+2}$	-	-	-	1.6482(108)	1.676(11)
$A_{vj} \times 10^{+2}$	-	-	-	3.7920(115)	3.8206(107)
ω_e	152.163530(490)	-	141.951647(316)	157.796220(387)	-
$\omega_e x_e$	0.2726923(204)	-	0.2748075(534)	0.2748075(534)	-
$\omega_e y_e \times 10^{+4}$	2.37572(490)	-	3.10879(674)	2.1705(242)	-
$p_e \times 10^{+3}$	-	-	-	7.02330(434)	7.0247(39)
$p_J \times 10^{+9}$	-	-	-	-3.1986(362)	-3.224(31)
$p_v \times 10^{+5}$	-	-	-	-4.2518(359)	-4.235(40)
$q_e \times 10^{+6}$	-	-	-	-1.885(341)	-1.373(328)
$q_J \times 10^{+12}$	-	-	-	12.53(211)	5.43(398)
$q_v \times 10^{+8}$	-	-	-	-	7.76(183)
$\gamma_e \times 10^{+3}$	2.53721(328)	2.53294(36)	-56.40837(416)	-	-
$\gamma_J \times 10^{+10}$	-4.051(220)	-3.82(11)	116.816(513)	-	-
$\gamma_v \times 10^{+5}$	-0.9994(437)	-1.124(11)	8.4308(763)	-	-
$\gamma_{vv} \times 10^{+7}$	-1.089(278)	-	-1.535(450)	-	-

Note. Numbers in parentheses represent two standard deviations in units of the last figure quoted.
(a) This work.
(b) Leach *et al.* (*1*).

TABLE 6
Comparison between the Pure Vibrational Parameters Obtained by Leach *et al.* (*1*) and the Ones Obtained from the Molecular Constants of Table 5

coeff.	This work	Leach *et. al* [1]
$\Delta v \times 10^4$	1.818849572(32)	1.81884943(3)
$\Delta\omega_e \times 10^0$	5.632690(806)	5.63482(13)
$\Delta\omega_e x_e \times 10^3$	-2.1152(738)	-2.5283(116)

Note. Numbers in parentheses represent two standard deviations in units of the last figure quoted.

of the $B^2\Sigma^+$ and $X^2\Sigma^+$ electronic states were described by a standard Hund's case b $^2\Sigma^+$ formula,

$$\begin{aligned} T &= T_v + B_v N(N+1) - D_v[N(N+1)]^2 \\ &\quad + H_v[N(N+1)]^3 + \cdots + \\ &\quad - \tfrac{1}{2}\gamma N \quad \text{for } e\text{-labeled levels, and} \\ &\quad - \tfrac{1}{2}\gamma(N+1) \quad \text{for } f\text{-labeled levels, with} \\ T_v &= T_e + \omega_e(v+1/2) - \omega_e x_e(v+1/2)^2 \\ &\quad + \omega_e y_e(v+1/2)^3 + \cdots \\ B_v &= B_e - \alpha_B(v+1/2) + \beta_B(v+1/2)^2 + \cdots \\ D_v &= D_e + \alpha_D(v+1/2) + \cdots \\ \gamma &= \gamma_e + \gamma_v(v+1/2) + \gamma_D N(N+1) + \cdots . \end{aligned} \quad [2]$$

The derived effective molecular constants for the ground state and for the $B^2\Sigma^+$ state, obtained in this preliminary analysis, are shown in Table 3. In this fit, the standard deviation of residual errors was less than 2.3×10^{-3} cm^{-1}.

The consistency of the derived molecular constants set for the ground electronic state with the ones for the same electronic state, as reported by Leach *et al.* (*1*), and also, the same order of magnitude for the standard deviations obtained in both analyses, have conducted a global analysis including the lines assigned in the present work combined with those published in (*1*) for the $C^2\Pi$–$X^2\Sigma^+$ band system. The Hamiltonian for the isolated $C^2\Pi$ electronic state is shown in Table 4. The vibrational dependence of the parameters was taken into account by a Dunham-type variation. For example,

$$\begin{aligned} T_v &= T_e + \omega_e(v+1/2) - \omega_e x_e(v+1/2)^2 \\ &\quad + \omega_e y_e(v+1/2)^3 + \cdots \\ A &= A_e + A_v(v+1/2) + A_{vv}(v+1/2)^2 + \cdots \\ B_v &= B_e - \alpha_B(v+1/2) + \beta_B(v+1/2)^2 + \cdots \\ D_v &= D_e + \alpha_D(v+1/2) + \cdots \\ p &= p_e + p_v(v+1/2) + p_J J(J+1) \\ &\quad + \cdots + p_{vv}(v+1/2)^2 + \cdots . \end{aligned} \quad [3]$$

In the final analysis, the $^2\Sigma^+$ electronic states were described in terms of Eq. [2].

Figure 6 shows a schematic diagram of the analyzed ground state vibrational and rotational data field. The complementarity of the spectroscopic data set obtained in this work and the one used by the authors (*1*) in their final analysis can be observed in the same figure. Figure 7 shows the range of the observed v' and J' in the upper $B^2\Sigma^+$ electronic state.

Table 5 summarizes the final values of the recommended molecular constants for the $B^2\Sigma^+$, $X^2\Sigma^+$, and $C^2\Pi$ electronic states, calculated in the global analysis described above. The values of the molecular constants obtained by Leach *et al.* (*1*) are quoted in the same table. The standard

TABLE 7
Comparison between the Theoretical Values of Transition Energies (in cm^{-1}) and the Ones Calculated in This Work

State	This work	Allouche *et. al* [5]	Törring *et. al* [2]
$\mathbf{B^2\Sigma^+}$	10427.02214(43)	10003	10160
$\mathbf{C^2\Pi}$	18188.49572(32)	21528	21220

Note. Numbers in parentheses represent two standard deviations in units of the last figure quoted.

TABLE 8

Comparison between the 24 Microwave Wavenumbers (in MHz) Assigned by Töring and Döbl (*17*) and the Ones Obtained from the Present Work Molecular Constants

v	N	J	$\nu_{obs.}$	$\nu_{calc.}$	$\nu_{obs.} - \nu_{calc.}$
0	55	54.5	89786.127	89785.221	0.906
0	55	55.5	89861.780	89861.021	0.759
0	64	63.5	104193.863	104192.878	0.985
0	64	64.5	104269.504	104268.635	0.869
0	65	64.5	105793.977	105792.981	0.996
0	65	65.5	105869.619	105868.736	0.883
1	55	54.5	89563.758	89562.273	1.028
1	55	55.5	89639.063	89638.224	0.839
1	64	63.5	103935.714	103934.592	1.122
1	64	64.5	104010.996	104010.043	0.953
1	65	64.5	105531.842	105530.720	1.122
1	65	65.5	105607.132	105606.168	0.964
2	55	54.5	89341.588	89340.482	1.106
2	55	55.5	89416.575	89415.661	0.914
2	64	63.5	103677.816	103676.584	1.232
2	64	64.5	103752.750	103751.727	1.023
2	65	64.5	105269.979	105268.740	1.239
2	65	65.5	105344.913	105343.874	1.039
3	64	63.5	103420.187	103418.862	1.325
3	64	64.5	103494.768	103493.681	1.087
4	64	63.5	103162.798	103161.565	1.233
4	64	64.5	103237.065	103235.913	1.152
5	64	63.5	102905.712	102904.259	1.453
5	64	64.5	102979.631	102978.422	1.209

Note. Differences $\nu_{obs.} - \nu_{calc.}$ are in MHz.

deviation was also less than 2.3×10^{-3} cm^{-1}. A strong similarity between the two sets of obtained molecular constants for the $X^2\Sigma^+$ and $C^2\Pi$ electronic states can be observed. The higher observed vibrational levels, v'' up to $v = 31$ in contrast with v'' up to $v = 12$ observed by Leach *et al.* (*1*), explain the presence of higher order terms (γ_B, β_D, $\omega_e y_e$, and γ_{vv}) for the $X^2\Sigma^+$ or $B^2\Sigma^+$ electronic states in the present analysis. The correction term $\omega_e y_e$ is significant in the isolated representation of the $C^2\Pi$ electronic state; for the other side, the terms q_J and β_D gave no significant contribution and were dropped in the final fit.

A last comparison between the constants obtained by Leach *et al.* (*1*) and the ones obtained in this work was done. Table 6 shows the pure vibrational terms obtained by Leach *et al.* (*1*) and obtained from the molecular constants calculated in this work. The significant difference between both $\Delta\omega_e x_e$ listed

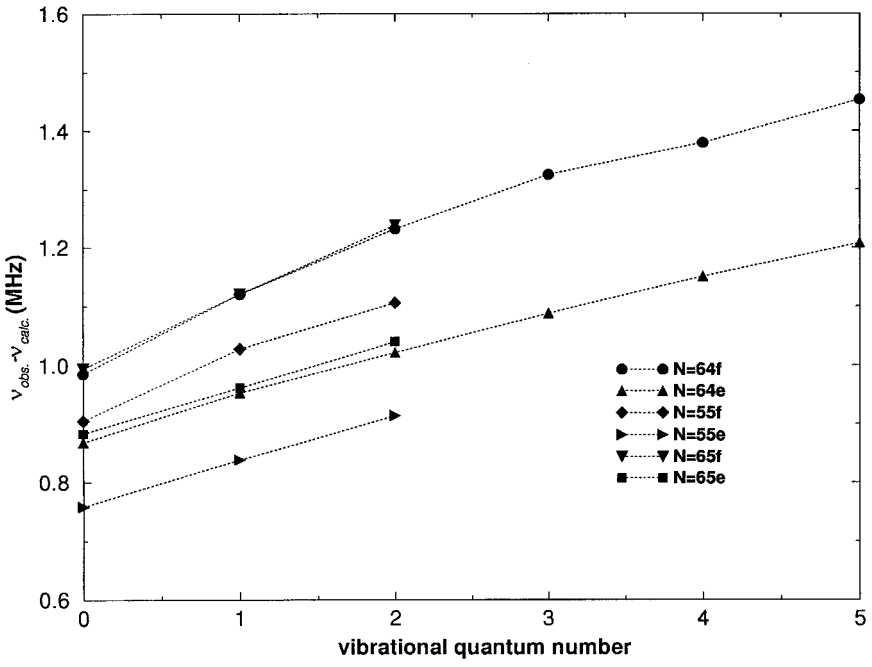

FIG. 8. Differences $\nu_{obs.} - \nu_{calc.}$ (in MHz) between the 24 microwave wavenumbers assigned by Töring and Döbl (*17*) and the ones obtained from the present work, molecular constants as function of v quantum number, e or f levels parity, and N quantum number.

values is due to the different data sets and representation Hamiltonians used in the performed analysis.

Table 7 shows the energy origins obtained in this work for the $B^2\Sigma^+$ and $C^2\Pi$ electronic states, and the theoretical values for the same constants derived from the model of ligand field approach (*5*) and from the model of electrostatic polarization (*2*). For the $B^2\Sigma^+$ electronic state, the difference between the theoretical and experimental transition energy values is less than 5% for the simpler model of ligand field approach and less than 2% for the model of electrostatic polarization. The difference is, however, larger than 15% for the two theoretical models in the case of the $C^2\Pi$ electronic state.

As remarked above, the high accuracy measurements of the $C^2\Pi$–$X^2\Sigma^+$ band system (*1*) were included in the final analysis, and, as they have the same order of uncertainty as the $B^2\Sigma^+$–$X^2\Sigma^+$ band system measurements, an unweighted fit of the global data set could be performed. The 24 microwave lines assigned by Töring and Döbl (*17*) (with an experimental uncertainty of 10^{-7} cm^{-1}) have not been included in the final analysis. Nevertheless, the global data set analyzed (including the $C^2\Pi$–$X^2\Sigma^+$ transitions) is reproduced with a smaller standard deviation than the one obtained by Leach *et al.* (*1*). Table 8 shows both the observed microwave transitions (*17*) and the same transitions obtained from the term energy values calculated in the present work. It is worth noting that the differences between these calculated values and the observed ones have a systematic behavior if the e or f levels parity, J and v values, are considered. This behavior is illustrated clearly in Fig. 8 and can be explained by a small error in the γ parameter indicated in (*17*) due to the unresolved hyperfine structure in the microwave measurements. Therefore, the inclusion of these data with a large weight could have led to biased calculated parameters.

V. CONCLUSION

Laser-induced fluorescence (LIF) and thermal emission, obtained from the chemiluminescent reaction Ba + I_2, combined with Fourier transform spectroscopy (FTS) have permitted the first spectroscopic study with rotational resolution of the $B^2\Sigma^+$–$X^2\Sigma^+$ band system of the BaI molecule. The data set published in (*1*) of the $C^2\Pi$–$X^2\Sigma^+$ band system of the BaI molecule was added to the present work data set and a global analysis of both $B^2\Sigma^+$–$X^2\Sigma^+$ and $C^2\Pi$–$X^2\Sigma^+$ band systems was performed. An improved set of molecular constants was calculated and described the observed transitions of both band systems with a standard deviation less than 2.3×10^{-3} cm^{-1}. In this work, the knowledge of the vibrational levels of the BaI ground state was extended from $v = 12$ (analyzed by Leach *et al.* (*1*) up to $v = 31$ (highest observed vibrational level). The vibrational constants T_e, ω_e, $\omega_e x_e$, and $\omega_e y_e$ were determined for each state, and for the first time, all observed transitions of both $B^2\Sigma^+$–$X^2\Sigma^+$ and $C^2\Pi$–$X^2\Sigma^+$ band systems were reproduced by a Hamiltonian which represents the energy levels of the three involved electronic states in an isolated form.

Current work is being done concerning the transitions from the $C^2\Pi$ state to the $A^2\Pi$, $B^2\Sigma^+$, and $A'\ ^2\Delta$ unobserved electronic state.

ACKNOWLEDGMENTS

This work is partially supported by CAPES/COFECUB (Brazil/France cooperation) 182/96. The authors are grateful to J. Chevillard for skillful help during the recording of the spectra.

REFERENCES

1. C. A. Leach, A. A. Tsekouras, and R. N. Zare, *J. Mol. Spectrosc.* **153,** 59–72 (1992).
2. T. Törring, W. E. Ernst, and S. Kindt, *J. Chem. Phys.* **90,** 4927–4932 (1989).
3. T. Törring, W. E. Ernst, and J. Kändler, *J. Chem. Phys.* **81,** 4614–4619 (1984).
4. S. F. Rice, H. Martin, and R. W. Field, *J. Chem. Phys.* **82,** 5023–5034 (1985).
5. A. R. Allouche, G. Wannous, and M. Aubert-Frécon, *Chem. Phys.* **170,** 11–22 (1993).
6. A. R. Allouche, Ph.D. thesis, Université Claude-Bernard Lyon I, 1993.
7. O. H. Walters and S. Barratt, *Proc. R. Soc. London, Series A* **118,** 120–137 (1928).
8. P. Mesnage, *Ann. Phys.* **12,** 5–9 (1939).
9. M. M. Patel and N. R. Shah, *Ind. Appl. Phys.* **8,** 681–682 (1970).
10. M. L. P. Rao, D. V. K. Rao, P. T. Rao, and P. S. Murty, *Fizika* **9,** 25–29 (1977).
11. R. S. Bradford, Jr., C. R. Jones, L. A. Southall, and H. P. Broida, *J. Chem. Phys.* **62,** 2060–2064 (1975).
12. M. A. Johnson, C. R. Webster, and R. N. Zare, *J. Chem. Phys.* **75,** 5575–5577 (1981).
13. M. A. Johnson and R. N. Zare, *J. Chem. Phys.* **82,** 4449–4459 (1985).
14. M. A. Johnson, C. Noda, J. S. McKillop, and R. N. Zare, *Can. J. Phys.* **62,** 1467–1477 (1984).
15. D. Zhao, P. H. Vaccaro, A. A. Tsekouras, C. A. Leach, and R. N. Zare, *J. Mol. Spectrosc.* **148,** 226–242 (1991).
16. C. A. Leach, J. R. Waldeck, C. Noda, J. S. McKillop, and R. N. Zare, *J. Mol. Spectrosc.* **146,** 465–492 (1991).
17. T. Töring and K. Döbl, *Chem. Phys. Lett.* **115,** 328–332 (1985).
18. C. R. Vidal and J. Cooper, *J. Appl. Phys.* **40,** 3370–3374 (1969).
19. C. Amiot, and J. Vergès, *Chem. Phys. Lett.* **185,** 310–312 (1991).
20. C. Amiot, M. Hafid, and J. Vergès, *J. Phys. B* **26,** L407–L412 (1993).
21. M. Hafid, C. Amiot, and J. Vergès, *Chem. Phys. Lett.* **210,** 45–49 (1993).
22. C. Amiot, M. Hafid, and J. Vergès, *J. Mol. Spectrosc.* **180,** 121–138 (1996).
23. O. Launila and P. Royen, *Mol. Phys.* **82,** 815–823 (1994).
24. A. Bernard, C. Effantin, E. Andrianavalona, J. Vergès, and R. F. Barrow, *J. Mol. Spectrosc.* **152,** 174–178 (1992).
25. Z. J. Jakubek and R. W. Field, *Phys. Chem. Lett.* **72,** 2167–2170 (1994).
26. C. M. Gittins, N. A. Harris, R. W. Field, J. Vergès, C. Effantin, A. Bernard, J. d'Incan, W. E. Ernst, P. Bündgen, and B. Engels, *J. Mol. Spectrosc.* **161,** 303–311 (1993).